Fabry–Pérot Optical Sensor and Portable Detector for Monitoring High-Resolution Ocular Hemodynamics

Jeong Oen Lee, Vinayak Narasimhan, Ashwin Balakrishna, Marcus R. Smith, Juan Du, David Sretavan, and Hyuck Choo, *Member, IEEE*

***Abstract*— Our understanding of ocular hemodynamics and its role in ophthalmic disease progression remains unclear due to the shortcomings of precise and on-demand biomedical sensing technologies. Here, we report high-resolution *in vivo* assessment of ocular hemodynamics using a Fabry–Pérot cavity-based micro-optical sensor and a portable optical detector. The designed optical system is capable of measuring both static intraocular pressure and dynamic ocular pulsation profiles in parallel. Through a dynamic intensity variation analysis method that improves sensing resolution by 3–4 folds, our system is able to extract systolic/diastolic phases from a single ocular pulsation profile. Using a portable detector, we performed *in vivo* studies on rabbits and verified that the ophthalmic parameters obtained from our optical system closely match with traditional techniques such as tonometry, electrocardiography, and photo-plethysmography.**

***Index Terms*— Optical sensing, portable detector, Fabry-Pérot interferometer, implantable sensor, intraocular pressure sensor, ocular hemodynamics.**

I. Introduction

As an organ, the eye requires constant perfusion during dynamic changes in blood pressure. While intraocular pressure (IOP) and ocular pulsation amplitude (OPA) are key ophthalmic parameters in glaucoma research, increasing evidence suggests that vascular abnormality and altered ocular hemodynamics also play important roles in the progression of open angle glaucoma [1], [2]. To date, various engineering efforts and clinical studies are underway to create an adequate examination platform for investigating ocular hemodynamics from a pathological point-of-view [3].

Typical ocular assessment and early studies on ocular hemodynamics were performed by using the Pascal Dynamic Contour Tonometer (DCT) [4]. Other techniques for monitoring ocular hemodynamics include high-resolution imaging instruments such as the Color Doppler imager [5], Laser Doppler Flowmeter [6] and Fourier-Domain Ocular Coherent Tomorgraphy [7]. However, these techniques require highly skilled, experienced technicians, and they are unsuitable for on-demand, continual, point-of-care (PoC) or self-monitoring applications [8].

In contrast, implantable device technologies [9]–[12] are able to collect detailed physiological data such as IOP from patients on-demand and have received growing attention in clinical ophthalmology [13]. Furthermore, significant advances have been made in the development of implantable photonic device technologies [14] thereby demonstrating unique advantages including battery-free operation, compact size, and high-sensitivity in biomedical applications. One way to achieve a miniaturized optical pressure sensor is combining a micro Fabry-Pérot (FP) interferometer [15]–[18] with pressure sensitive membrane and subsequently mapping the spectral-shift to the different pressure states. Similarly, photonic crystals [19], [20] and optical strain sensors [21] were also suggested for optical IOP sensing applications [22], [23].

However, while most of emerging implantable sensors and optical readout approaches focus on the measurement of static IOP, they have never demonstrated the detection of (i) dynamic ocular pulsation profiles and (ii) multiple ophthalmic parameters such as IOP, OPA and arterial parameters in parallel through implantable system platform. In order to obtain clinically important information included in ocular hemodynamics, optically-driven implantable ocular devices should provide sufficiently high pressure-sensitivity and time-resolution coupled with efficient signal processing.

II. System Overview

To address the aforementioned needs, we have used an implantable FP cavity-based micro-optomechanical sensor

Manuscript received November 11, 2018; revised January 9, 2019; accepted January 19, 2019. Date of publication February 1, 2019; date of current version March 12, 2019. This work was supported in part by the National Institutes of Health under Grant EY024582, in part by the Heritage Medical Research Institute, in part by the National Research Foundation of Korea (NRF-2013R1A6A3A03026384), and in part by the Powell Foundation Award. *(Corresponding author: Hyuck Choo.)*

J. O. Lee was with the California Institute of Technology, Pasadena, CA 91125 USA. He is now with the National Institute of Health, Bethesda, MD 20852 USA (e-mail: jeongoen.lee@nih.gov).

V. Narasimhan is with the Department of Medical Engineering, California Institute of Technology, Pasadena, CA 91125 USA (e-mail: vnarasim@caltech.edu).

A. Balakrishna is with the Department of Electrical Engineering, California Institute of Technology, Pasadena, CA 91125 USA (e-mail: abalakri@caltech.edu).

M. R. Smith is with Microsmith, Inc., Pine Grove, CA 95665 USA (e-mail: ismith9999@aol.com).

J. Du and D. Sretavan are with the Department of Ophthalmology, University of California at San Francisco, San Francisco, CA 94143 USA (e-mail: juan.du@ucsf.edu; david.sretavan@ucsf.edu).

H. Choo is with the Department of Electrical Engineering, California Institute of Technology, Pasadena, CA 91125 USA, with the Department of Medical Engineering, California Institute of Technology, Pasadena, CA 91125 USA, and also with the Samsung Advanced Institute of Technology, Suwon 16678, South Korea (e-mail: hchoo@caltech.edu).

Digital Object Identifier 10.1109/LPT.2019.2896840

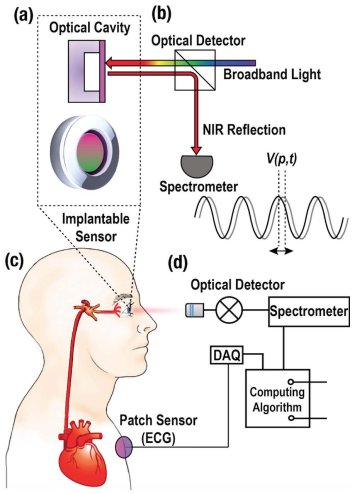

Fig. 1. *In vivo* ocular pulsation monitoring system. (a) Schematic of an implantable optomechanical cavity-based sensor (top) and a tilted 3D illustration of the sensor (bottom). (b) Simplified diagram of the remote optical detector. (c) A test subject with (d) the detection system.

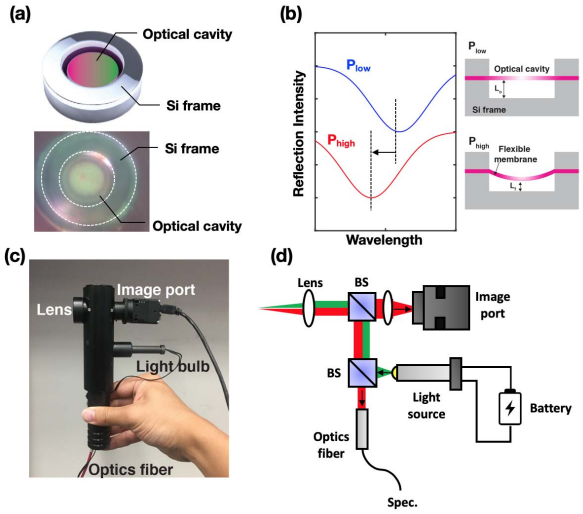

Fig. 2. All-optical intraocular sensor implant and assessment system. (a) Implantable optomechanical sensor. (b) Optical spectrum of the optomechanical sensor in low and high pressures. (c) Handheld optical detector. (d) Design scheme and components of the handheld detector.

(**Fig. 1a**) and a convenient handheld detector (**Fig. 1b**) for fast and accurate measurements of dynamic ocular pulsation. Previously, we reported only static IOP monitoring for glaucoma through a wavelength-shift ($\Delta\lambda$) method [24], [25] that relies on the shift of the FP cavity resonance based on IOP. In this work, however, exploiting a newly developed dynamic intensity variation (DIVA) analysis technique, the pressure sensitivity is improved 3-4-folds compared to our previous method. As a result, the system allows us to accurately discern the ocular pulsation pattern in the spectral measurements and subsequently extract the systolic and diastolic phases from each ocular pulse. As the ocular pulse represents blood pressure fluctuations that propagate through the ophthalmic artery (**Fig. 1c**), we validated our ocular hemodynamic assessment through a comparison with conventional cardiovascular monitoring devices such as ECG and PPG (**Fig. 1d**). In parallel, static IOP and OPA were concurrently extracted with the $\Delta\lambda$ method, enabling multi-parameter monitoring from a single optical spectral acquisition.

III. Device and Detection System

The implantable microscale optical sensor consists of two halves – (i) a flexible and deformable silicon nitride (Si_3N_4) membrane and (ii) a reflective mirror-like silicon (Si) surface both fabricated through silicon micromachining techniques (**Fig. 2a**) [24]. The two halves are separated by a recess and hermetically sealed together to form a FP cavity with diameters range from 600-900 μm. When the ambient pressure changes, i.e. IOP spikes, the flexible Si_3N_4 membrane deforms, thereby shifting the resonance spectrum of the cavity. This shift is detected through reflection spectroscopy by illuminating the sensor with noninvasive broadband light (**Fig. 2b**).

The miniaturized handheld and portable optical detector is shown in **Fig. 2c**. The compact handheld framework is inspired by a monocular ophthalmoscope. The schematic of the detecting system is shown in **Fig. 2d**. Powered by commercial batteries (AAA 1.5V, Duracell Inc., USA), it incorporates miniaturized, low-cost optical components, including a dichroic short pass filter (<750nm, Edmund Optics Inc., USA), an objective lens (f = 35.0 mm, Ø1", Thorlabs Inc., USA), and a tungsten-filament light source, all housed in a lightweight plastic casing weighing 159 g. An optical fiber connected to the detector relays the reflected light to a commercial broadband VIS-NIR mini-spectrometer (780-1180 nm, MAYA 2000 Pro-NIR, Ocean Optics, USA) that collects the resonance spectra of the sensor implant. The manipulation of the portable detector is simple, similar to using magnifying lenses that are commonly available in clinics and home, and a user can easily locate the implanted sensor through either an eyepiece or an attached camera.

IV. Results and Analysis

We characterized the fabricated micro-optical sensor under a pressure-ramp (0 – 40 mmHg) on a benchtop test [24]. After the benchtop characterization and surgical implantation, we validated *in vivo* functionality of the system using the $\Delta\lambda$ method first. Then, a comparison study between the $\Delta\lambda$ method and the DIVA technique was carried out.

Reflected spectra were obtained from the sensor implanted in the anterior chamber of a New Zealand white rabbit using the portable handheld detector (**Fig. 3a** and **b**). High signal-to-noise ratio (SNR ~17 dB) *in vivo* resonance spectra from the sensor are shown in **Fig. 3c**. In the measurement corresponding to **Fig. 3c**, we processed collected spectra (n = 37) with high SNR and obtained a mean IOP value of 14.1 mmHg. This IOP baseline was consistent with rebound tonometry measurements taken concurrently for reference (14 mmHg ± 1.8 mmHg, TonoVet, Icare, USA). Next, by tracking the dynamic $\Delta\lambda$ over time with the sampling frequency of 100 Hz, a periodically fluctuating waveform upon the time-variant IOP profile can be plotted as shown in **Fig. 3d**. The OPA is the pressure

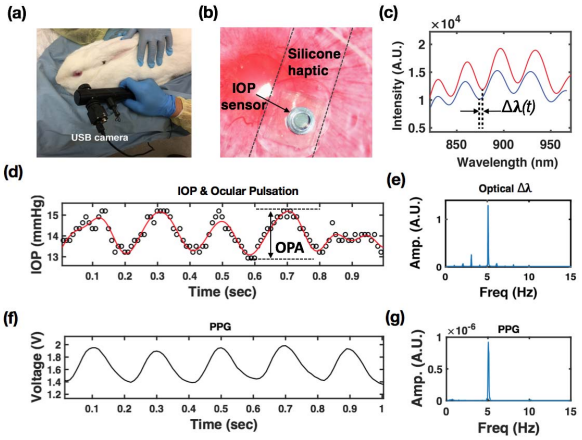

Fig. 3. *In vivo* ocular pulsation measurement produced using wavelength-shift ($\Delta\lambda$). (a) *In vivo* sensor measurement using the portable detector. (b) An implanted optomechanical sensor delivered into an anterior chamber of an awaken rabbit eye. A diameter of IOP sensor is 900 μm; dotted line showing the boundary of transparent silicone haptic (2 mm × 10 mm × 0.1 mm). The flexible haptic with our IOP sensor is placed on the iris. (c) Representative optical spectra showing cavity resonance shift in two different IOPs. SNR is 17 dB. Fig.4 (d) IOP and OPA profile computed from the optical resonance detection. Black dots indicate raw data and solid-red line indicates the fitted curve. (e) FFT spectra of the OPA profile measured by optical detecting system. (f) Reference PPG measurement indicating cardiac-driven hemodynamics. (g) FFT spectra of the PPG profile.

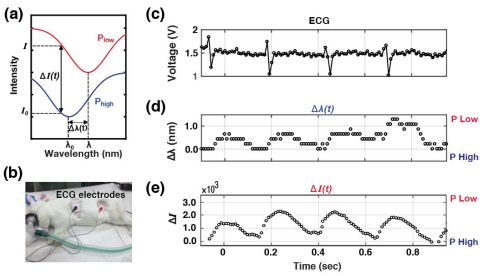

Fig. 4. High-resolution ocular pulsation profiling using the DIVA method. (a) Cavity resonance shift: the intensity change provides higher DR than the wavelength shift for a given pressure change. (b) ECG measurement setup. (c) recorded ECG profile for 1 second. (d) Low-resolution discretized cavity resonance detection through wavelength-shift in the sub-1-nm wavelength regime. (e) High-resolution continuous intensity detection with the same raw data used in (b). Note that the baseline intensity (I_0) and the wavelength (λ_0) are set at the local maximum pressure point (P_{high}). Thus, the relative intensity-shift ($\Delta I = I - I_0$) and the wavelength-shift ($\Delta\lambda = \lambda - \lambda_0$) are positive ($\Delta I > 0$ and $\Delta\lambda > 0$) when the relative pressure decreases from P_{high} to P_{low}.

difference between the minimum (or diastolic) and maximum (or systolic) values of the pulsatile IOP pattern [4]. The pulsatile waveform indicates an OPA of 1.8 – 2.2 mmHg. The OPA frequency of 4.9 Hz is obtained using Fast Fourier Transform (FFT) analysis (**Fig. 3e**). To confirm if this frequency component is induced by cardiac activities, we conducted a reference blood-flow measurement using a photoplethysmography (PPG) device. **Fig. 3f** and **g** show that the OPA frequency is in good agreement with the cardiac hemodynamics.

Further resolution improvement can be achieved by the DIVA method which measures relative intensity fluctuation (ΔI) in the resonance profile instead of detecting the wavelength location. The substantial sensitivity improvement using the intensity-based analysis can be understood with an illustration of the cavity resonance shift (**Fig. 4a**). This plot represents the resonance wavelength-shift property of the IOP sensor. Normally, the optical resonance spectrum of the sensor cavity shifts in the transverse direction along the x-axis as a function of pressure, and the blue and red curves indicate two different pressure states driven by ocular perfusion. Given our spectrometer-based detection scheme, the DIVA method can offer higher a detection resolution (DR, resolution/mmHg) than the wavelength-shift method for a given pressure change. This is attributed to $\Delta I/\Delta P$ (photon count/mmHg) per minimum intensity resolution of the spectrometer ($N_I \approx 150$ photon counts corresponding to the floor noise) being greater than $\Delta\lambda/\Delta P$ (nm/mmHg) per minimum wavelength resolution of spectrometer ($N_\lambda = 0.2$ nm).

To compare the proposed DIVA method to the original $\Delta\lambda$ method, we performed the same optical spectrum measurements with a synchronized electrocardiogram (ECG) recording (**Fig. 4b**). The ECG profile representing the electrical signal of the heart was recorded by attaching three probing electrodes on the rabbit's chest and collecting the data using a microcontroller (AD8232, Arduino, USA). The rabbit was anesthetized to minimize artifacts due to motion for reliable ECG recording (**Fig. 4c**). For a fair comparison, the optical spectra were first acquired, and the same raw data was analyzed using the DIVA ΔI and the $\Delta\lambda$ methods, as shown in **Fig. 4d** and **e** respectively. The oscillatory pattern within both optical measurements corresponded to the ocular pulsation profile had an amplitude of ∼1 mmHg and a frequency of 4 Hz. The frequency of this oscillation agrees with that of the concurrently taken ECG measurements that directly relates to cardiac cycles.

In the sub-1-nm regime of the $\Delta\lambda$ detection method (**Fig. 4d**), the acquired data points become highly discretized, making the wavelength detection scheme ineffective for visualizing subtle fluidic fluctuations that arise as a result of ocular hemodynamics. The best mini-spectrometer available today offers a wavelength resolution $\Delta\lambda$ of 0.2 nm (roughly the size of the diffraction grating). As shown in **Fig. 4d and e**, the $\Delta\lambda$ detection scheme offered only 4-5-levels of resolution per 1.0 mmHg, while the DIVA method provides 12-20 levels, resulting in a 3-4-fold resolution improvement. In addition, the DIVA method allows for near real-time data processing of the same optical spectra.

Next, we applied the DIVA method to analyze *in vivo* resonance spectra, and we were able to clearly observe the periodic pulsation patterns in intensity for 10 seconds without any post signal processing (**Fig. 5a**). In the intensity profile, the low-frequency saw-tooth-like pattern (or the pattern with a pseudo-periodic dip that appears almost every 2.5 s) was attributed to the respiratory motion of the animal. The high-frequency component (∼4 Hz) occurring between adjacent respiratory motions corresponds to the ocular pulsation profile. After removing the low-frequency components using a digital band-pass filter (pass band: 3–12 Hz), the ocular pulsation profile becomes distinguishable as shown in **Fig. 5b**. In the zoomed-in plot (**Fig. 5c**), systolic and diastolic phases of the ocular pulse are clearly discernible. The average time difference between the systolic and diastolic peak is 0.061 ± 0.022 sec

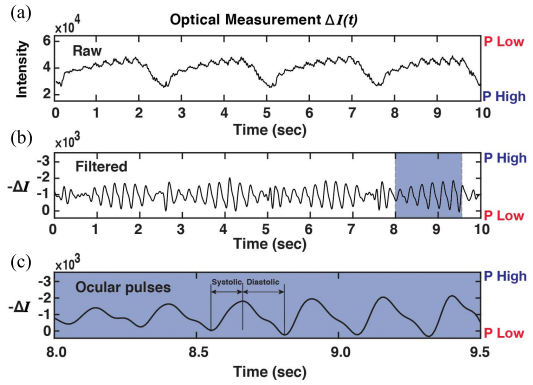

Fig. 5. Systolic and diastolic phase classification using DIVA method. (a) Time-dependent *in vivo* intensity fluctuation during ocular assessment at the probing wavelength of 850 nm. (b) Filtered intensity profile processed by a digital bandpass filter (3-12Hz). The negative intensity change ($\Delta I < 0$) indicates a pressure increase from P_{low} to P_{high} ($\Delta P > 0$). (c) Zoomed-in intensity profile for 1.5 second presenting *in vivo* ocular pulsation profile and systolic/diastolic phases.

(number of pulses n = 52). As a result, following the digital volume pulse method [26], the arterial stiffness index was calculated to be 4.53 ± 0.58 m/s, and the critical error was 1.5%. These values match well with those reported in literature [27].

V. Conclusion

In this work, we report an all-optical approach for monitoring ocular hemodynamics at high-resolution. The system consists of a micro-optomechanical sensor and a portable handheld detector. Compared with traditional ophthalmic examination tool, such as DCT, our approach allows comfortable characterization of fast-paced IOP fluctuations in detail and collection of various vital ophthalmic parameters. To faithfully characterize ocular hemodynamics that manifest as small-amplitude IOP fluctuations with fast temporal variations, we developed a DIVA method to improve the detection sensitivity of the system by 3–4-fold over the wavelength-shift-based IOP mapping algorithm, thereby resolving and enabling the proper analysis of systolic and diastolic phases within a single ocular pulsation profile. During *in vivo* testing, we successfully obtained multiple physiological parameters including IOP, OPA, and cardiac phases on ocular pulsation profile. Through this multi-parameter analysis and with advantages in accuracy, robustness, portability and cost-effectiveness, we hope to use this platform to better elucidate role of ocular hemodynamics fluctuations in the progression of glaucoma.

References

[1] N. Yüksel, V. L. Karabaş, A. Arslan, A. Demirci, and Y. Çağlar, "Ocular hemodynamics in pseudoexfoliation syndrome and pseudoexfoliation glaucoma," *Ophthalmology*, vol. 108, no. 6, pp. 1043–1049, 2001.

[2] J. Caprioli and A. L. Coleman, "Blood pressure, perfusion pressure, and glaucoma," *Amer. J. Ophthalmol*, vol. 149, no. 5, pp. 704–712, 2010.

[3] E. M. Hoffmann, F.-H. Grus, and N. Pfeiffer, "Intraocular pressure and ocular pulse amplitude using dynamic contour tonometry and contact lens tonometry," *BMC Ophthalmol.*, vol. 4, no. 1, p. 4, 2004.

[4] C. Kaufmann, L. M. Bachmann, Y. C. Robert, and M. A. Thiel, "Ocular pulse amplitude in healthy subjects as measured by dynamic contour tonometry," *Arch. Ophthalmol.*, vol. 124, no. 8, pp. 1104–1108, 2006.

[5] H. J. Kaiser, A. Schötzau, and J. Flammer, "Blood-flow velocities in the extraocular vessels in normal volunteers," *Amer. J. Ophthalmol*, vol. 122, no. 3, pp. 364–370, 1996.

[6] I. Kimura, K. Shinoda, T. Tanino, Y. Ohtake, Y. Mashima, and Y. Oguchi, "Scanning laser Doppler flowmeter study of retinal blood flow in macular area of healthy volunteers," *Brit. J. Ophthalmol.*, vol. 87, no. 12, pp. 1469–1473, 2003.

[7] P. Li *et al.*, "Visualization of the ocular pulse in the anterior chamber of the mouse eye *in vivo* using phase-sensitive optical coherence tomography," *J. Biomed. Opt.*, vol. 19, no. 9, 2014. Art. no. 090502

[8] A. Harris, L. Kagemann, R. Ehrlich, C. Rospigliosi, D. Moore, and B. Siesky, "Measuring and interpreting ocular blood flow and metabolism in glaucoma," *Can. J. Ophthalmol.*, vol. 43, no. 3, pp. 328–336, 2008.

[9] G. Chen *et al.*, "A cubic-millimeter energy-autonomous wireless intraocular pressure monitor," in *IEEE Int. Solid-State Circuits Conf. (ISSCC) Dig. Tech. Papers*, Feb. 2011, pp. 310–312.

[10] E. Y. Chow, A. L. Chlebowski, and P. P. Irazoqui, "A miniature-Implantable RF-wireless active glaucoma intraocular pressure monitor," *IEEE Trans. Biomed. Circuits Syst.*, vol. 4, no. 6, pp. 340–349, Dec. 2010.

[11] S. Melki, A. Todani, and G. Cherfan, "An implantable intraocular pressure transducer: Initial safety outcomes," *JAMA Ophthalmol.*, vol. 132, no. 10, pp. 1221–1225, 2014.

[12] K.-S. Shin *et al.*, "Development of novel Implantable intraocular pressure sensors to enhance the performance *in vivo* tests," *J. Microelectromech. Syst.*, vol. 24, no. 6, pp. 1896–1905, 2015.

[13] K. Mansouri and T. Shaarawy, "Continuous intraocular pressure monitoring with a wireless ocular telemetry sensor: Initial clinical experience in patients with open angle glaucoma," *Brit. J. Ophthalmol.*, vol. 95, no. 5, pp. 627–629, 2011.

[14] M. Humar, S. J. J. Kwok, M. Choi, A. K. Yetisen, S. Cho, and S.-H. Yun, "Toward biomaterial-based implantable photonic devices," *Nanophoton*, vol. 6, no. 2, pp. 414–434, 2017.

[15] Y. Zhu and A. Wang, "Miniature fiber-optic pressure sensor," *IEEE Photon. Technol. Lett.*, vol. 17, no. 2, pp. 447–449, Feb. 2005.

[16] Y. Bai, Y. Qi, Y. Dong, and S. Jian, "Highly sensitive temperature and pressure sensor based on Fabry-Perot interference," *IEEE Photon. Technol. Lett.*, vol. 28, no. 21, pp. 2471–2474, Nov. 2016.

[17] Y. Tian, N. Wu, X. Zou, Y. Zhang, K. Barringhaus, and X. Wang, "A study on packaging of miniature fiber optic sensors for *in-vivo* blood pressure measurements in a swine model," *IEEE Sensors J.*, vol. 14, no. 3 pp. 629–635, Mar. 2014.

[18] M. Li, M. Wang, and H. Li, "Optical MEMS pressure sensor based on fabry-Perot interferometry," *Opt. Exp.*, vol. 14, no. 4, pp. 1497–1504, 2006.

[19] Y.-P. Wong, S. Lorenzo, and O. Solgaard, "Design and fabrication of monolithic Photonic crystal fiber acoustic sensor," *IEEE Sensors J.*, vol. 18, no. 19, pp. 7826–7832, Oct. 2018.

[20] T. Karrock and G. Martina, "Pressure sensor based on flexible photonic crystal membrane," *Biomed. Opt. Exp.*, vol. 6, no. 12, pp. 4901–4911, 2015.

[21] J. Fernandes, Y. H. Kwon, J.-J. Kim, H. Liu, H. Jiang, "High contrast grating based strain sensor for intraocular applications," *J. Microelectromech. Syst.*, vol. 27, no. 4, pp. 599–601, 2018.

[22] A. Phan, P. Truong, J. Trumpp, and F. E. Talke, "Design of an optical pressure measurement system for intraocular pressure monitoring," *IEEE Sensors J.*, vol. 18, no. 1, pp. 61–68, Jan. 2018.

[23] P.-J. Chen *et al.*, "Implantable micromechanical parylene-based pressure sensors for unpowered intraocular pressure sensing," *J. Micromech. Microeng.*, vol. 17, no. 10, pp. 1931–1938, 2007.

[24] J. O. Lee *et al.*, "A microscale optical implant for continuous *in vivo* monitoring of intraocular pressure," *MicroSyst. NanoEng.*, vol. 3, Dec. 2017, Art. no. 17057.

[25] V. Narasimhan *et al.*, "Multifunctional biophotonic nanostructures inspired by the longtail glasswing butterfly for medical devices," *Nature Nanotechnol.*, vol. 13, pp. 512–519, Apr. 2018.

[26] G. D. Simonetti, U. Eisenberger, I. P. Bergmann, F. J. Frey, and M. G. Mohaupt, "Pulse contour analysis: A valid assessment of central arterial stiffness in children?" *Pediatric nephrol.*, vol. 23, no. 3, pp. 439–444, 2008.

[27] S. Hayashi, S. Obara, M. Murakawa, A. Hazama, M. Kusanagi, and S.-I. Katsuda, "To what extent does aortic pulse wave velocity estimate early atherosclerosis in Kurosawa and Kusanagi-hypercholesterolemic rabbits?" *Hypertension Res.*, vol. 34, no. 5, pp. 559–564, 2011.